Exact solutions to steady radial flow in a porous medium with variable permeability

Y. Nec[1] and G. Huculak[2]
[1)] *Department of Mathematics and Statistics, Thompson Rivers University, Kamloops, British Columbia, Canada, V2C 0C8; correspondence should be directed to ynec@tru.ca*
[2)] *GNH Consulting Ltd., Delta, British Columbia, Canada, V4M 2S6*

A wide class of exact solutions to equations of steady flow of ideal gas in a porous medium is obtained in a planar annular domain comprising sectors of distinct permeabilities. The formulation involves an unconventional Sturm-Liouville problem. The class also admits solutions to configurations with respective distinct generation rates. The solutions are expected to be applicable to landfill gas (LFG) or natural gas extraction. The breaking of axial symmetry enables realistic modelling of the radius of influence for both horizontal and vertical wells. The analysis proves that the well's reach would have an azimuthal dependence in any problem with a heterogeneous medium. Therefore it is suggested that the concept of radius of influence as perceived today be revised.

I. INTRODUCTION

Studies of flow through porous media date as far back as mid nineteenth century and are underpinned by the matrix resistance to flow, quantified through the concept of permeability. A seminal description of the factors salient in its estimation was given by Carman [1]. In the vast majority of applications the permeability is taken as a single effective value to circumvent analytical difficulties. Over the years a small number of breakthrough studies reported solutions with a non-constant permeability. The first appears to be Cheng [2], solving an incompressible flow, where the square root of the conductivity k (a parameter better suited for hydraulic problems, but mathematically equivalent to permeability) is taken to be a harmonic function, i.e. $\Delta\sqrt{k} = 0$, enabling a solution via Green's function. Several explicit forms of $k(x,y)$ are analysed, interestingly leading to radial functional shapes typical of flow in cylindrical coordinates: $\ln r$ associated with the source or sink potential flow as well as Bessel functions of r. Thereupon Chandrasekhara [3] obtains similarity solutions for a mixed convection boundary layer with heat transfer subject to an exponential variation of permeability for a plate as well as over a wedge[4]. Rees and Pop [5] revisit the system studied in Chandrasekhara [3] 15 years later, giving an asymptotic solution. The next results are by Hamdan and Kamel [6], who use a quadratic permeability function in the analysis of convection in a channel, and Capone, Gentile, and Hill [7], studying a fluid with a prescribed dependence of density on temperature penetrating a medium with a generic non-smooth permeability function. Around the same time Ciriello *et al.* [8] studied the flow of an incompressible fluid under gravity with the permeability varying as a power law, possibly fractional; the flow between two coaxial stationary[9] and rotating[10] cylinders was solved with either linear or quadratic radial variation of permeability; and Verma and Datta [11] solved the flow past a porous sphere, whose permeability is a function of radial distance.

The paucity of analytical studies attests to the difficulties associated with the mathematical analysis of systems with variable permeability. The current contribution reports new exact solutions with a discontinuous piecewise constant permeability function $k(\theta)$ for the flow of an ideal gas in polar geometry. To the best of the authors' knowledge, this is the only study in existence to date on an azimuthal variation of permeability. The results are expected to be applicable in environmental gas problems such as landfill gas flow or extraction of natural gas. For instance, in the problem of a perforated horizontal landfill well it was shown that the derivatives in the longitudinal direction were small, so that within a cross-section the flow could be approximated as planar[12].

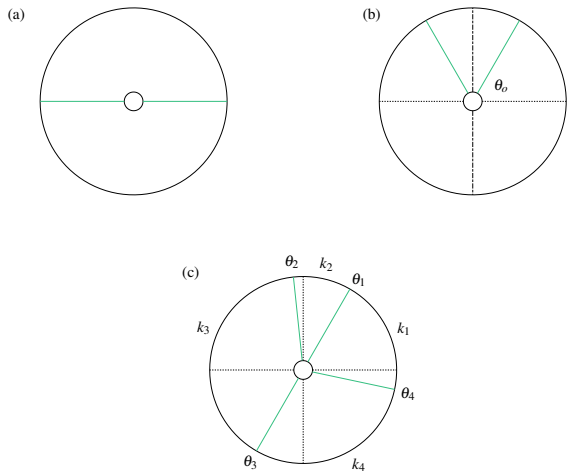

FIG. 1. Domain configurations and notation

II. GEOMETRY AND FLOW EQUATIONS

Consider a planar annular domain represented in polar coordinates (r,θ) as $[r_P\ r_X]\times(-\pi\ \pi]$, where r_P and r_X stand for inner and outer radii. The annulus is divided into N sectors filled with porous media of constant permeabilities k_s, $s = \{1,\ldots,N\}$, such that $k_s \neq k_{s+1}$ for any $1 \leqslant s < N$ and $k_N \neq k_1$. For brevity notation of the type $(\,\cdot\,)_s = (\,\cdot\,)_{s+1}$ will tacitly imply the wrapping condition $(\,\cdot\,)_{N+1} = (\,\cdot\,)_1$ throughout via the statement $1 \leqslant s \leqslant N$. The indexing of contiguity rays θ_s and

sector permeabilities k_s is counter-clockwise with the first ray $\theta_1 \geqslant 0$ and k_1 assigned to the sector immediately preceding θ_1. Consult the example in figure 1(c).

In environmental applications such as landfill gas or natural gas flow it is reasonable to expect that effective values can be assigned to given regions, computed according to Carman [1] or otherwise estimated. A steady flow field of ideal gas through a porous medium entails conservation of mass[13]

$$\frac{1}{r}\frac{\partial}{\partial r}(r\rho u) + \frac{1}{r}\frac{\partial}{\partial \theta}(\rho v) = C, \tag{1a}$$

and balance of momentum, alias Darcy's law[14]

$$\boldsymbol{u} = -\frac{k}{\mu}\nabla p = -\frac{k}{\mu}\left(\frac{\partial p}{\partial r}, \quad \frac{1}{r}\frac{\partial p}{\partial \theta}\right)^{\mathrm{T}}, \tag{1b}$$

wherein $\boldsymbol{u} = (u,\ v)^{\mathrm{T}}$ is the velocity vector with u and v radial and azimuthal components respectively, and the permeability k is a function of θ. Fluid pressure is denoted by p and density – by ρ, related through the ideal gas equation $p = \rho RT$, where R is the gas constant and T – temperature. For the purpose of this derivation it is assumed the system is under thermal equilibrium and the temperature field can be represented by an effective value, as is the case in landfill gas flow[15]. C is the generation rate and μ – fluid viscosity. If the gas is a mix, R is given by $R = R_o \Big/ \sum_i x_i M_i$, where R_o is the universal gas constant, and x_i, M_i are the components' molar fractions and weights. Then μ is computed according to Davidson [16]. Equation (1b) does not include velocity components induced by the gravitational force. A conjunction of circumstances, with boundary conditions being a prominent factor, might render gravity non-negligible[17]. Notwithstanding, this assumption served to obtain analytical solutions in vertical[18], horizontal and spherical geometry[19] with a uniform permeability, and is inevitable within the current more complicated framework.

As a first step consider the generation rate to be identical in all sectors. Combining all of the above yields a system of equations for the pressure p_s in each sector of permeability k_s:

$$\frac{\partial}{\partial r}\left(k_s r\frac{\partial p_s^2}{\partial r}\right) + \frac{\partial}{\partial \theta}\left(\frac{k_s}{r}\frac{\partial p_s^2}{\partial \theta}\right) = -2\mu RTCr, \quad s = \{1, \ldots, N\}. \tag{2}$$

To cast (2) into a dimensionless form select characteristic scales $\bar{r}$ and $\bar{p}$ and map $p_s \longmapsto \bar{p}p_s$, $r \longmapsto \bar{r}r$. Then $k_s \longmapsto k_s\bar{r}^2$ and $C \longmapsto C/\tilde{\mu}$ define the corresponding non-dimensional permeability and generation rate, where $\tilde{\mu} = \mu RT/\bar{p}^2$ is a compound that will be used throughout for brevity. Hence

$$\frac{\partial}{\partial r}\left(k_s r\frac{\partial p_s^2}{\partial r}\right) + \frac{\partial}{\partial \theta}\left(\frac{k_s}{r}\frac{\partial p_s^2}{\partial \theta}\right) = -2Cr, \quad s = \{1, \ldots, N\}, \tag{3a}$$

where all quantities are non-dimensional. In order to effect correct matching of solutions in the different sectors, the following conditions must hold on the contiguity rays θ_s: continuity of pressure (and consequently its square and radial velocity u)

$$p_s^2(r, \theta_s) = p_{s+1}^2(r, \theta_s), \quad 1 \leqslant s \leqslant N, \tag{3b}$$

and azimuthal velocity v

$$k_s \left.\frac{\partial p_s^2}{\partial \theta}\right|_{\theta_s^-} = k_{s+1} \left.\frac{\partial p_{s+1}^2}{\partial \theta}\right|_{\theta_s^+}, \quad 1 \leqslant s \leqslant N. \tag{3c}$$

The continuity of v is imbedded in (3a), as equation (3c) ensues by integration of (3a) over the interval $(\theta_s - \varepsilon,\ \theta_s + \varepsilon)$, taking the limit $\varepsilon \longrightarrow 0$ and using the fact that p is continuous. Equation (3c) implies that the function p^2 belongs to the C^0 differentiability class, i.e. continuous, but not differentiable with respect to θ on the rays θ_s. Each sector must be of a sufficient volume to constitute an isotropic porous medium. System (3) cannot be used where the permeability k exhibits a strong continuous variation in the azimuthal direction requiring a fine discretisation for adequate representation. To complete the problem, boundary conditions on the annulus must be set. These can be of either Dirichlet

$$p(r_P, \theta) = p_P, \qquad p(r_X, \theta) = p_X \tag{4a}$$

or Neumann type

$$-\frac{r_{P,X}}{2\tilde{\mu}}\int_{-\pi}^{\pi} k \left.\frac{\partial p^2}{\partial r}\right|_{r_{P,X}} \mathrm{d}\theta = f_{P,X}, \tag{4b}$$

where $p_{P,X}$ and $f_{P,X}$ are specified pressure and normal flux values at radii $r_{P,X}$ (all dimensionless). Whilst (4) fulfil the formal requirements of the problem statement, later on in the interest of attaining exact solutions these boundary conditions will be modified slightly. In the problems of landfill gas or natural gas extraction $p_P < p_X$, so that the fluid flows inwards. Nonetheless the solution class given below allows for outward flow in the same degree.

III. BASIC SOLUTION

This section develops the basic solution in a single sector that is essential in construction of the full class of exact solutions to (1) in the annular domain. The subscript s is omitted for simplicity. First observe that substituting

$$p^2 \overset{\text{def}}{=} P(r, \theta) = \tilde{P}(r, \theta) - \frac{C}{2k}r^2 \tag{5}$$

in (3a) gives a homogeneous equation for $\tilde{P}$, soluble with the technique of separation of variables:

$$r\frac{\partial}{\partial r}\left(r\frac{\partial \tilde{P}}{\partial r}\right) + \frac{\partial^2 \tilde{P}}{\partial \theta^2} = 0. \tag{6}$$

Writing $\tilde{P}(r, \theta) = A(r)B(\theta)$ and separating r and θ dependent terms in (6) results in

$$\left(rA'\right)'\frac{r}{A} = -\frac{B''}{B} = \alpha^2, \tag{7}$$

wherein α is a constant, generally complex, and neither A nor B vanishes. Since in this context one is interested in periodic solutions, $\alpha^2 \geqslant 0$, so in fact $\alpha \in \mathbb{R}$. Thus the solution

space of B is spanned by $\{\sin(\alpha\theta),\, \cos(\alpha\theta)\}$ when $\alpha \neq 0$ and $\{1,\ \theta\}$ if $\alpha = 0$. The solution $B = \theta$ is not periodic and must be discarded. The respective solution space of A is spanned by $\{r^{\alpha},\ r^{-\alpha}\}$ when $\alpha \neq 0$ and $\{1,\ \ln r\}$ if $\alpha = 0$.

Limiting this basic derivation to configurations symmetric across the vertical will ultimately allow to write the solutions for unrestricted configurations more elegantly. Thus imposing $B\big(\pi/2+\theta\big) = B\big(\pi/2-\theta\big)$ results in the eigenvalues $\alpha = 1+2n$ and $\alpha = 2n$ for the sine and cosine eigenfunctions respectively with $n \geqslant 0$ an integer. This preliminary eigenfunction basis is orthogonal and complete (subject to the symmetry condition). Hence by linearity of (3a), introducing arbitrary constants a_{in} and b_{in}, $i = \{1,2\}$, and combining all foregoing solutions in (5) yields

$$P = -\frac{C}{2k}r^2 + b_{10} + b_{20}\ln r + \sum_{n=0}^{\infty}\Big(a_{1n}r^{2n+1} + a_{2n}r^{-(2n+1)}\Big)\sin\big((2n+1)\theta\big) + \sum_{n=1}^{\infty}\Big(b_{1n}r^{2n} + b_{2n}r^{-2n}\Big)\cos\big(2n\theta\big). \tag{8}$$

Hereinafter this solution is used to construct a flow field in an annular domain. In a conventional Sturm-Liouville problem the coefficients in (8) would have served to satisfy boundary conditions, and completeness of the eigenfunction basis would have been imperative to allow for generic boundary functions. By contrast, herein these coefficients must be set so as to create a valid flow field with the pressure and radial velocity continuous on the contiguity rays. This curtails the genericity of acceptable boundary conditions, whereby the ensuing eigenfunction basis, albeit orthogonal, is not complete.

Remark 1 *For $n = 1$ the functional shape of the term r^{2n} in the single sector solution (8) matches the generation term in (5). This coincidence is crucial to the existence of exact solutions in an annular domain.*

Remark 2 *For a solution not encumbered by symmetry across the vertical two additional sequences would be present, corresponding to* $\sin(2n\theta)$ *and* $\cos\big((2n+1)\theta\big)$. *However, if there is symmetry across a different diametral line, solution (8) can be rotated accordingly, as the governing equations (1) are invariant under the mapping $\theta \longmapsto \theta + \theta_*$ for an arbitrary rotation angle θ_*.*

IV. SEMI-CIRCULAR CONFIGURATION

This is the simplest annular solution available in the class endowed by (8) and of twofold value. One, it elucidates which structural aspects of (8) are imperative to satisfy (3b) and (3c), thereby creating a valid annular solution. Two, it is forthwith likely to find application in the area of environmental gas extraction. For instance, in the problem of landfill gas flow toward a horizontal well[12,19] planar analytical flow solutions use an effective permeability value, whilst experience indicates that the natural settlement of the waste lamina significantly affects the deeper part of the landfill[20,21]. Therefore it will be beneficial to assign distinct permeability values to the top and bottom halves thereof. In the problem of a vertical well a similar division of landfill waste or soil in a natural gas extraction site into two hollow semi-cylinders of distinct permeability might prove equally useful where material differences in matrix properties are present, such as fractured rock[22].

Returning the attention to the planar domain, by remark 2 the division line might be set at horizontal without loss of generality. The configuration is shown in figure 1(a). All coefficients in (8) as well as the function P now bear a parenthesised superscript indicating the relevant sector, respectively $(\,\cdot\,)^{(1)}$ and $(\,\cdot\,)^{(2)}$ for bottom and top. Equations (3b) and (3c) must hold on contiguity rays $\theta_s = 0, \pi$, but it is immediate that both angles give identical equations. Equating coefficients of terms of distinct radial dependence yields

$$b_{i_0}^{(1)} = b_{i_0}^{(2)}, \quad i = \{1,2\}, \tag{9a}$$

$$k_1 a_{in}^{(1)} = k_2 a_{in}^{(2)}, \quad i = \{1,2\},\ n \geqslant 0, \tag{9b}$$

$$b_{2_n}^{(1)} = b_{2_n}^{(2)}, \quad n \geqslant 1; \qquad b_{1_n}^{(1)} = b_{1_n}^{(2)}, \quad n \geqslant 2;$$

$$b_{1_1}^{(1)} = b_{1_1}^{(2)} + \frac{C}{2}\left(\frac{1}{k_1} - \frac{1}{k_2}\right). \tag{9c}$$

Implementing boundary conditions of the Dirichlet type on the inner and outer top semi-circle (e.g. imposed well pressure p_P and a higher pressure $p_X > p_P$ on the outer boundary)

$$P^{(2)}(r_P,\theta) = p_P^2, \quad P^{(2)}(r_X,\theta) = p_X^2 \tag{10a}$$

gives $a_{in}^{(2)} = 0\ \forall n \geqslant 0$ and $b_{in}^{(2)} = 0\ \forall n \geqslant 1$ for $i = \{1,2\}$. A similar result follows from an identical condition on the inner semi-circle in conjunction with a zero flux outside (sealed boundary):

$$P^{(2)}(r_P,\theta) = p_P^2, \quad \left.\frac{\partial P^{(2)}}{\partial r}\right|_{r_X} = 0. \tag{10b}$$

For $n = 0$ by (9a) it is possible to define $b_{i_0}^{(s)} \overset{\text{def}}{=} b_{i0}$, whereupon conditions (10a) and (10b) give

$$b_{20} = \left(p_X^2 - p_P^2 + \frac{C}{2k_2}\left(r_X^2 - r_P^2\right)\right)\Big/ \ln\frac{r_X}{r_P} \tag{11a}$$

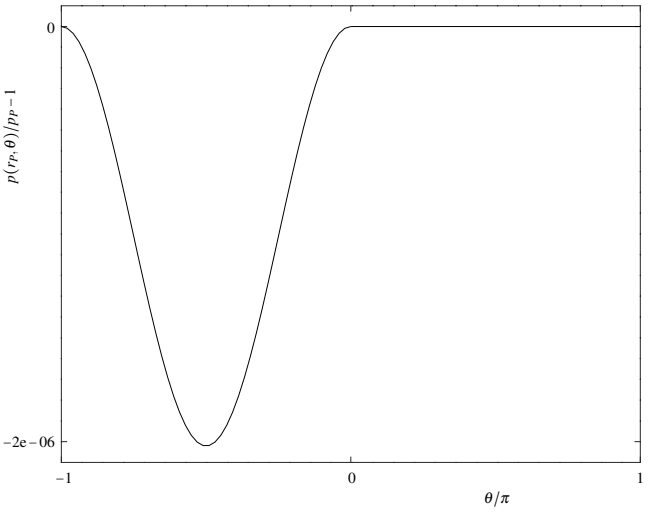

FIG. 2. Relative difference between pressure as given by exact solution (12) and boundary value p_P. $k_1 = 1\mathrm{e}-08\mathrm{m}^2$, $k_2 = 1\mathrm{e}-06\mathrm{m}^2$. All other parameters listed in appendix A

and

$$b_{20} = \frac{C}{k_2} r_X^2 \tag{11b}$$

respectively, and for both

$$b_{10} = p_P^2 + \frac{C}{2k_2} r_P^2 - b_{20} \ln r_P. \tag{11c}$$

Therefore for $0 \leqslant \theta \leqslant \pi$

$$P^{(2)} = -\frac{C}{2k_2} r^2 + b_{10} + b_{20} \ln r, \tag{12a}$$

and for $-\pi \leqslant \theta \leqslant 0$

$$P^{(1)} = \frac{C}{2} r^2 \left\{ \left(\frac{1}{k_1} - \frac{1}{k_2} \right) \cos(2\theta) - \frac{1}{k_1} \right\} + b_{10} + b_{20} \ln r, \tag{12b}$$

where b_{i0} are given by (11).

Remark 3 *The matching conditions (3b) and (3c) in conjunction with the boundary conditions of the top semi-annulus determine the state on the boundaries of the bottom one. This elicits the question to what extent this departs from the boundary pressure and flux values prescribed in (10). The answer lies in the magnitude of the oscillatory term in (12b). Figure 2 depicts the comparison for the case of a typical medium sized landfill, illustrating that the difference is negligible even when k_1 and k_2 differ by two orders of magnitude, and the generation rate value is purposely taken very large (appendix A). In other configurations the magnitude of the undesired term might be more tangible, however exact solutions often come with limitations, and here these stem from the required continuity of the radial velocity u across contiguity rays.*

Remark 4 *For the application of a horizontal landfill well it stands to reason to impose boundary conditions on the top sector, where there is control of the surface state. However, it is equally possible to implement the boundary conditions on the bottom sector if the problem formulation calls for that.*

Remark 5 *More complicated boundary conditions involving higher azimuthal frequencies are possible. The usual Fourier series expansion technique will furnish the coefficients. Herein this option is foregone, since as explained in remark 3, the qualitative impact thereof is negligible in the example problem of the horizontal landfill well; and in practice the implementation of such conditions is unlikely.*

V. TWO UNEQUAL SECTORS

To solve a configuration of the type shown in figure 1(b) a similar analysis is performed, however more caution is required. The technical detail appears in appendix B. Implementation of boundary conditions (10) as they are is impossible, however for a slight modification

$$p(r_{P,X}, \theta) = p_{P,X} \sqrt{1 + \frac{C r_{P,X}^2}{2k_2 p_{P,X}^2} \frac{\cos(2\theta)}{\cos(2\theta_o)}}\ , \tag{13}$$

where a calculation as in figure 2 proves the additional terms have negligible qualitative impact, one gets

$$P^{(s)} = \frac{C}{2k_s} r^2 \left(\frac{\cos(2\theta)}{\cos(2\theta_o)} - 1 \right) + b_{10} + b_{20} \ln r,$$

$$s = \{1, 2\}, \qquad \theta_{s-1} \leqslant \theta \leqslant \theta_s, \tag{14}$$

with θ_o denoting the angle contiguity rays make with the horizontal line as marked in figure 1(b), and b_{i0}, $i = \{1, 2\}$, as in (11). Note the elegant symmetry between the two sectors' solutions. In fact it is possible to achieve the same symmetry in (12) by "transferring" the term with k_2 in (12b) to (12a), but then the boundary condition on the top semi-annulus will have to be as in (13). Fortunately the contribution to the total radial flux on either boundary (or any circle concentric with the annulus) vanishes, as can be seen by integrating

$$\int_{-\pi}^{\pi} \rho u r \, \mathrm{d}\theta = -\frac{r}{2\tilde{\mu}} \int_{-\pi}^{\pi} k(\theta) \frac{\partial P}{\partial r} \, \mathrm{d}\theta, \tag{15}$$

where a full cycle integral on $\cos(2\theta)$ will yield zero.

Remark 6 *The temporary restriction of vertical symmetry is relaxed in any two sector configuration as in remark 2: for a symmetry line tilted off the vertical at angle θ_* the rotation $P^{(s)}(r, \theta) \longmapsto P^{(s)}(r, \theta - \theta_*)$ provides the desired result.*

Remark 7 *Solution (14) is invalid for $\theta_o = \pi/4$. There exists no steady flow solution for this case, as equations (3b) and (3c) cannot be satisfied. Consult appendices B and D for detail.*

VI. *N* ARBITRARY SECTORS

Implementing the lessons on structural aspects imperative to attain an exact solution and relaxing the symmetry constraints, the solution for a generic configuration as in figure 1(c) is of the form

$$P^{(s)} = \frac{C}{2k_s} r^2\Big(a^{(s)}\sin(2\theta) + b^{(s)}\cos(2\theta) - 1\Big) + b_{10} + b_{20}\ln r,$$

$$\theta_{s-1} \leqslant \theta \leqslant \theta_s, \qquad s = \{1, \ldots, N\}. \tag{16a}$$

The full derivation appears in appendix C. The coefficients $a^{(s)}$ and $b^{(s)}$ satisfy an (almost) block bi-diagonal linear system of equations of size $2N\times 2N$:

$$\begin{pmatrix} \mathfrak{A}_1 & \mathfrak{B}_1 & & & & \\ & \mathfrak{A}_2 & \mathfrak{B}_2 & & & \\ & & \ddots & \ddots & & \\ & & & \mathfrak{A}_{N-1} & \mathfrak{B}_{N-1} & \\ \mathfrak{B}_N & & & & \mathfrak{A}_N & \end{pmatrix} \begin{pmatrix} \boldsymbol{c}_1 \\ \boldsymbol{c}_2 \\ \vdots \\ \boldsymbol{c}_{N-1} \\ \boldsymbol{c}_N \end{pmatrix} = \begin{pmatrix} \boldsymbol{r}_1 \\ \boldsymbol{r}_2 \\ \vdots \\ \boldsymbol{r}_{N-1} \\ \boldsymbol{r}_N \end{pmatrix}, \tag{16b}$$

where

$$\mathfrak{A}_s = \begin{pmatrix} \sin(2\theta_s) & \cos(2\theta_s) \\ \cos(2\theta_s) & -\sin(2\theta_s) \end{pmatrix}, \tag{16c}$$

$$\mathfrak{B}_s = \begin{pmatrix} -k_r^{(s)}\sin(2\theta_s) & -k_r^{(s)}\cos(2\theta_s) \\ -\cos(2\theta_s) & \sin(2\theta_s) \end{pmatrix}, \tag{16d}$$

$$\boldsymbol{c}_s = \begin{pmatrix} a^{(s)} \\ b^{(s)} \end{pmatrix}, \quad \boldsymbol{r}_s = \begin{pmatrix} 1 - k_r^{(s)} \\ 0 \end{pmatrix}, \quad k_r^{(s)} = \frac{k_s}{k_{s+1}}, \tag{16e}$$

and as before the index $s+1$ wraps back to 1 for $s = N$, and is also the reason for the block $\mathfrak{B}_N$ appearing in the bottom left corner, breaking the perfect bi-diagonality. For most configurations the determinant of the matrix in (16b) is not zero, begetting a unique solution. For $N = 2$ and $\theta_2 = \pi - \theta_1$ solution (14) is recovered upon inversion thereof (the algebra is somewhat tedious, but elementary). Similarly to the case of two sectors, the boundary conditions on one sector (denote it by s_*) must be

$$p(r_{P,X}, \theta)\Big/ p_{P,X} = \sqrt{1 + \frac{Cr_{P,X}^2}{2k_{s*}p_{P,X}^2}\Big(a^{(s*)}\sin(2\theta) + b^{(s*)}\cos(2\theta)\Big)},$$

$$\theta_{s_*-1} \leqslant \theta \leqslant \theta_{s_*}, \tag{17}$$

and the state on the boundaries of the remaining sectors is determined by continuity therewith.

VII. DISTINCT GAS GENERATION RATE

All foregoing solutions can be summarily extended to accommodate distinct generation rates C_s in each of the sectors. The continuity of azimuthal velocity – equation (3c) – is not affected. For two semi-circular sectors equations (12) become

$$P^{(2)} = -\frac{C_2}{2k_2} r^2 + b_{10} + b_{20}\ln r, \tag{18a}$$

$$P^{(1)} = \frac{r^2}{2}\left\{\left(\frac{C_1}{k_1} - \frac{C_2}{k_2}\right)\cos(2\theta) - \frac{C_1}{k_1}\right\} + b_{10} + b_{20}\ln r. \tag{18b}$$

For two unequal sectors the counterpart of (14) is

$$P^{(s)} = \frac{r^2}{2}\left(b_s\frac{\cos(2\theta)}{\cos(2\theta_o)} - \frac{C_s}{k_s}\right) + b_{10} + b_{20}\ln r,$$

$$\theta_{s-1} \leqslant \theta \leqslant \theta_s, \qquad s = \{1, 2\}, \tag{19a}$$

where the coefficients b_s are given by

$$b_1 = \left(\frac{C_2}{k_2} - \frac{C_1}{k_1}\right)\frac{k_2}{k_1 - k_2}, \quad b_2 = \left(\frac{C_2}{k_2} - \frac{C_1}{k_1}\right)\frac{k_1}{k_1 - k_2}. \tag{19b}$$

For N sectors system (16) morphs into

$$P^{(s)} = \frac{r^2}{2}\frac{C_s}{k_s}\Big(a^{(s)}\sin(2\theta) + b^{(s)}\cos(2\theta) - 1\Big) + b_{10} + b_{20}\ln r,$$

$$\theta_{s-1} \leqslant \theta \leqslant \theta_s, \qquad s = \{1, \ldots, N\}, \tag{20a}$$

with the coefficients $a^{(s)}$ and $b^{(s)}$ satisfying a system of the same form as (16b), upon amending the matrix $\mathfrak{B}_s$ to read

$$\mathfrak{B}_s = \begin{pmatrix} -k_r^{(s)}\sin(2\theta_s) & -k_r^{(s)}\cos(2\theta_s) \\ -c_r^{(s)}\cos(2\theta_s) & c_r^{(s)}\sin(2\theta_s) \end{pmatrix}, \tag{20b}$$

wherein $c_r^{(s)} = C_{s+1}\big/C_s$ is the generation ratio of adjacent sectors, and the quondam permeability ratio is redefined as $k_r^{(s)} = \big(k_s\big/k_{s+1}\big)c_r^{(s)}$. Then the expressions given for the right hand side vectors $\boldsymbol{r}_s$ in (16) remain correct, but contain the redefined values of $k_r^{(s)}$.

Remark 8 *Following the algebra outlined in appendix D for $N = 2$ gives*

$$\det\Big(\mathfrak{B}_1^{-1}\mathfrak{A}_1 - \mathfrak{A}_2^{-1}\mathfrak{B}_2\Big) = -\Big(c_r^{(2)} - k_r^{(2)}\Big)^2\sin^2\Big(2(\theta_2 - \theta_1)\Big).$$

Therefore the additional degrees of freedom accorded in this section do not affect the determinant roots altogether and the singularity corresponding to one sector being right angled still stands. For singularity analysis consult appendix D.

VIII. APPLICATION TO A HORIZONTAL LANDFILL GAS WELL

Hitherto the assumption of axial symmetry was inevitable if an analytical solution was to be obtained for this problem[19], whilst in reality the pressure isocontours are evidently not circular. Some numerical studies broke this symmetry, with approaches ranging from the introduction of multiple layers of permeability decreasing with depth[23] and to drawing attention to the fact that gravity might not be negligible, as it affects not only the balance of vertical momentum, but also the Neumann boundary conditions[17]. The new exact solutions found here admit a realistic asymmetric distribution of the pressure isocontours, as is illustrated below.

Another modelling aspect these solutions inadvertently ameliorate is the implementation of boundary conditions on the outermost circumference of the domain. Pervading the literature in this area, boundary conditions follow the mathematical convention of Dirichlet and Neumann type conditions. The only justified condition is that of zero flux on a sealed boundary, however that conforms to reality only in a rectangular domain. Mathematical convention aside, in this problem the desirable state would be not to have to specify a boundary condition anywhere, but on fully sealed boundaries or surfaces open to the atmosphere. Since a circular outermost boundary could only approximate a realistic domain of an inscribing square (the corners are expected to have minor qualitative effect due to proximity to the boundary), the circular boundaries cannot be modelled as fully sealed. Therefore the fact that the solutions given herein require a boundary condition only in one sector (chosen as the top one), renders the modelling more realistic. Top sectors of an angle less than π will further reduce the undesired prescription of pressure on a boundary that does not coincide with the surface.

A. Two sectors

Figure 3(a) depicts the flow field with permeabilities differing by one order of magnitude. There are two attributes of note. One, the open bottom contours are almost normal to the boundary, indicating little radial flow, a physical feature previously sought in numerical simulations with a rectangular domain,[17,23] and now attained analytically. Two, the marked saddle point implies the existence of a stagnation point about two thirds of the landfill depth below the well. The notion of the radius of influence, whilst being a well understood quantity in hydraulic wells, in the problem of landfill gas flow remains moot. The scarce methods suggested to define and calculate it appeared to overestimate reality and furthermore were fraught with complexity that hindered their implementation in practice. The solutions given here are accessible to field operators and yield the radius of influence graphically as the distance of the largest closed contour from the well. Usage of these estimates in modelling of specific landfills is a subject of future studies with the aim to determine whether they represent reality more faithfully.

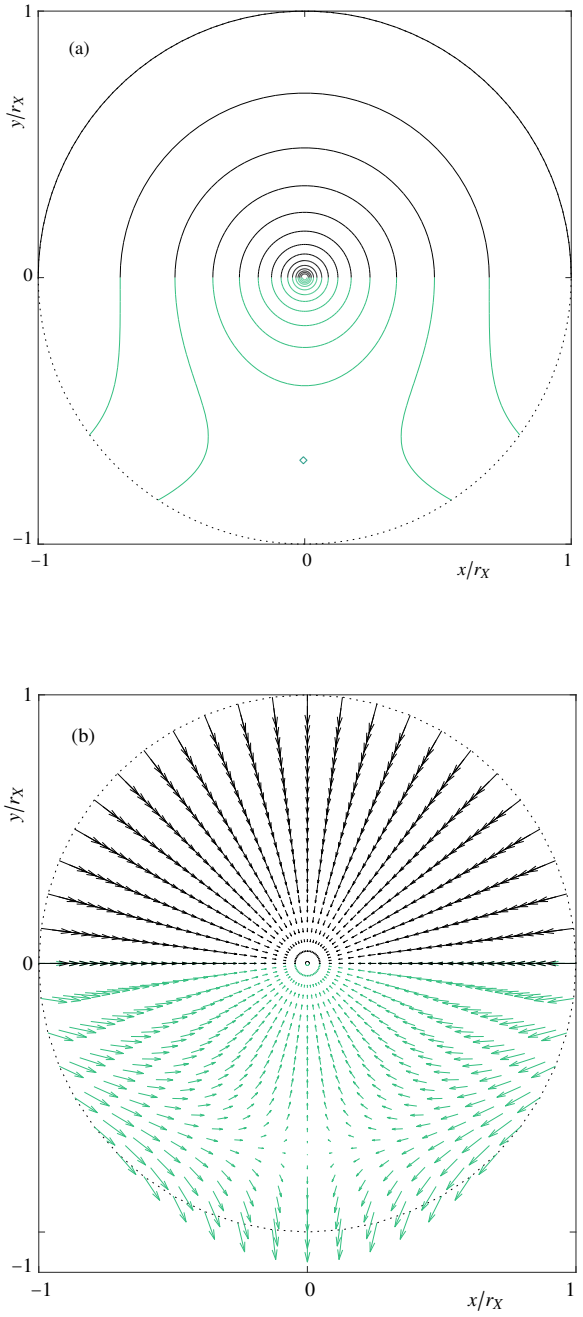

FIG. 3. (a) Pressure contours by (12) at 15 equally distributed values in the range $[p_P\ p_X]$. $\theta_1 = 0$, $\theta_2 = \pi$. $k_1 = 1\mathrm{e}-07\mathrm{m}^2$ (green / grey), $k_2 = 1\mathrm{e}-06\mathrm{m}^2$ (black). The diamond marks the stagnation point. All other parameters listed in appendix A. (b) Respective velocity vector orientation by (1b). Note the arrows' length is not to scale and they represent local flow direction only

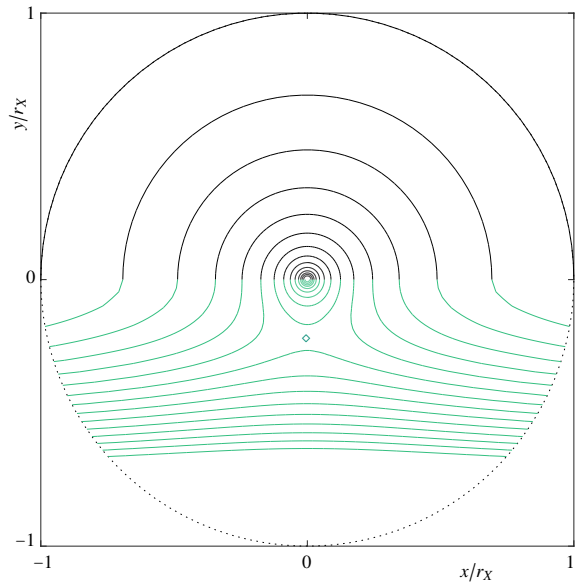

FIG. 4. Pressure contours by (12) at 15 equally distributed values in the range $[p_P\ p_X]$. $\theta_1 = 0$, $\theta_2 = \pi$. $k_1 = 1\mathrm{e}-08\mathrm{m}^2$ (green / grey), $k_2 = 1\mathrm{e}-06\mathrm{m}^2$ (black). The diamond marks the stagnation point. All other parameters listed in appendix A

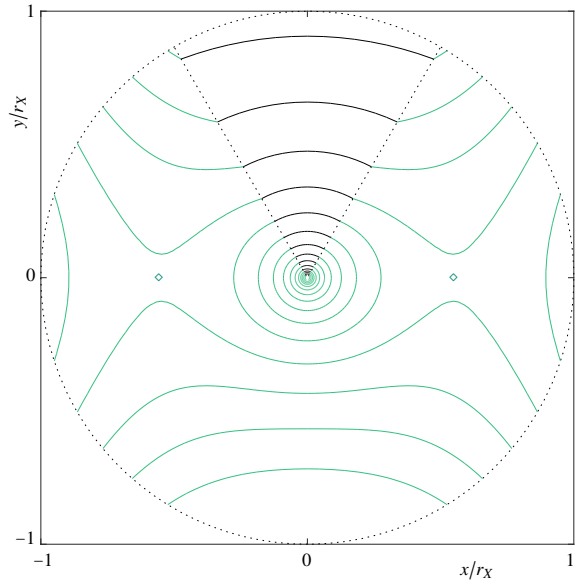

FIG. 5. Pressure contours by (14) at 15 equally distributed values in the range $[p_P\ p_X]$. $\theta_1 = \pi/3$, $\theta_2 = 2\pi/3$. $k_1 = 1\mathrm{e}-07\mathrm{m}^2$ (green / grey), $k_2 = 1\mathrm{e}-06\mathrm{m}^2$ (black). The diamonds mark the stagnation points. All other parameters listed in appendix A

In the landfill gas field pressure distribution is the natural variable to depict: the flow is controlled by exertion of vacuum, regulations set high pressure thresholds, and the landfill operator's primary responsibilities are to monitor the highest pressure value and distance where the induced suction dissipates. The contour density in figure 3(a) hints at a fully fledged boundary layer behaviour (in the mathematical sense) near the well. Figure 3(b) depicts the corresponding velocity vector field, however the arrows are not to scale. The absolute velocity spans at least two orders of magnitude with the highest values obtained at the well, where the visual resolution of the polar grid diminishes, rendering uniform arrow length scale impossible. Furthermore, as evinced in figure 2, the azimuthal and radial components of the velocity are also disparate in magnitude, making an accurate integration of streamlines a computationally difficult task that requires custom treatment similar to rigid differential equations. Therefore pressure distribution is the only feasible way to visualise this flow field without omitting information or introducing distortion as in figure 3(a), and the qualitative features of the velocity field are illative by (1b).

Figure 4 gives the same flow field, but with permeabilities differing by two orders of magnitude. This disparity renders the bottom sector's resistance so high that it effectively stops the flow toward the well. The green / grey contours that continue the black ones and are not closed, turn sharply to become almost horizontal and as before, intersect the boundary almost perpendicularly. The stagnation point is now located closer to the well. Underneath that point the contours quickly level into virtually horizontal lines, demonstrating the well's failure to extract gas generated in that region. Out of the 15 contours plotted, 9 lie below the stagnation point, corresponding to the 9 closed contours proximate to the well and indicating that below the stagnation point the gas flows away from the well with a velocity similar to its flow toward the well in the immediate vicinity thereof. This flow field invites the inference that overly compacted waste beneath the well will result in severely diminished collection from that sector, with the gas trapped and seeking to circle upwards into the medium of lesser resistance. This state should be avoided if the suction imposed at the well is to be used to its full potential. Somewhat counter-intuitively, compacting the waste in the top sector will yield a more efficient collection.

Figure 5 exemplifies the flow field with a smaller top sector. This situation is relevant when (a) new waste is added at the top part of the landfill; and (b) the sides are compacted to be of a similar permeability as the older settled waste beneath the well; and (c) the sector immediately above the well is left in loose fettle to avoid damage to the well from heavy machinery. There are two stagnation points that indicate the radius of influence. In this instance the largest closed contour would be quite oblate, implying that the concept of the radius of influence as adopted from hydraulic wells is not adequate here: the well's reach might vary significantly with the azimuthal angle.

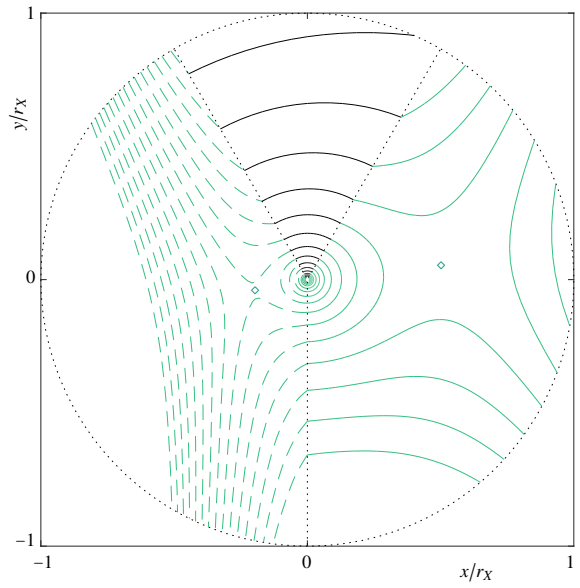

FIG. 6. Pressure contours by (16) at 15 equally distributed values in the range $[p_P\ p_X]$. $\theta_1 = \pi/3$, $\theta_2 = 2\pi/3$, $\theta_3 = 3\pi/2$. $k_1 = 1\mathrm{e}-07\mathrm{m}^2$ (green / grey), $k_2 = 1\mathrm{e}-06\mathrm{m}^2$ (black), $k_3 = 1\mathrm{e}-08\mathrm{m}^2$ (dashed green / grey). The diamonds mark the stagnation points. All other parameters listed in appendix A

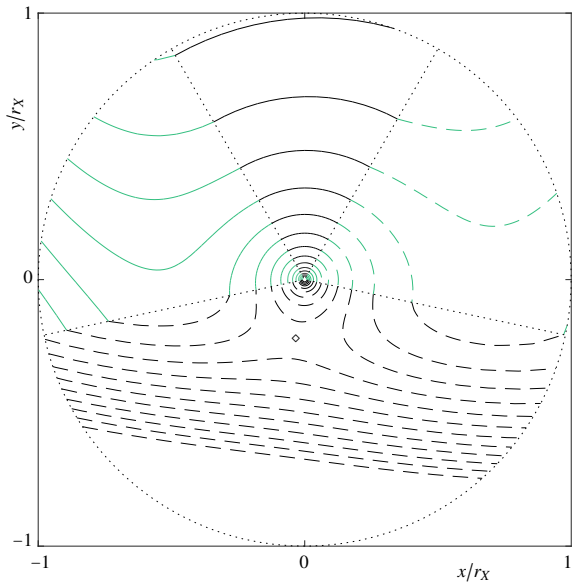

FIG. 7. Pressure contours by (16) at 15 equally distributed values in the range $[p_P\ p_X]$. $\theta_1 = \pi/3$, $\theta_2 = 2\pi/3$, $\theta_3 = 16\pi/15$, $\theta_3 = 29\pi/15$. $k_1 = 1\mathrm{e}-07\mathrm{m}^2$ (dashed green / grey), $k_2 = 1\mathrm{e}-06\mathrm{m}^2$ (black), $k_3 = 5\mathrm{e}-08\mathrm{m}^2$ (green / grey), $k_4 = 1\mathrm{e}-08\mathrm{m}^2$ (dashed black). The diamond marks the stagnation point. All other parameters listed in appendix A

B. Three sectors

Figure 6 depicts a landfill with three sectors such that the following conditions hold: the left and right sectors respectively contain dense (e.g. household garbage / organic matter) and large fragment size waste (e.g. demolition and land clearing debris); both aforementioned sectors are newly compacted, whereas the sector above the well is not. Note the extreme asymmetry of the well's influence, suggesting that poor control of waste density and ensuing heterogeneity in the medium permeability is likely to result in severely diminished collection effectiveness.

C. Four sectors

Figure 7 models a field that is perhaps the most common operational regime of a real landfill cell: (a) bottom sector bearing the highest density due to natural settlement; and (b) side sectors of distinct permeabilities due to content or filling time or compacting differences, but within the same order of magnitude; and (c) not compacted top sector. There is only one stagnation point located in the bottom sector. Within the other three sectors the permeability values were chosen to span two orders of magnitude, yet no additional saddle points appeared. This is an encouraging evidence of a sufficient leeway permissible in the control that should be exercised over the compaction of waste in the top part of the landfill. One feature of note that was not accomplished in any of the foregoing configurations is that there are open contours with endpoints located on left and right sides of the landfill throughout the depth of the domain. This implies that the modelling is a good qualitative approximation of the flow field in a realistic rectangular domain, because with a straight top surface and constant pressure thereon, and sufficiently far away from the well, the contours must conform to the shape of the boundary.

IX. DISCUSSION

The theory developed in this study pertains to the weakly compressible flow of ideal gas through a porous medium in domains of axisymmetric geometry, but admitting azimuthal variation of permeability, thereby breaking the axial symmetry. The exact solutions are expected to be applicable in the analysis of horizontal and vertical extraction wells of landfill gas or natural gas. The long-standing difficulties to control the landfill gas flow in the face of waste spatial heterogeneity and changes with degradation observed in the field, were given a mathematical explanation. In contrast to most analytical solutions in this area – bar the fully symmetric ones presented in Wise and Townsend [19] – the formulae fortuitously

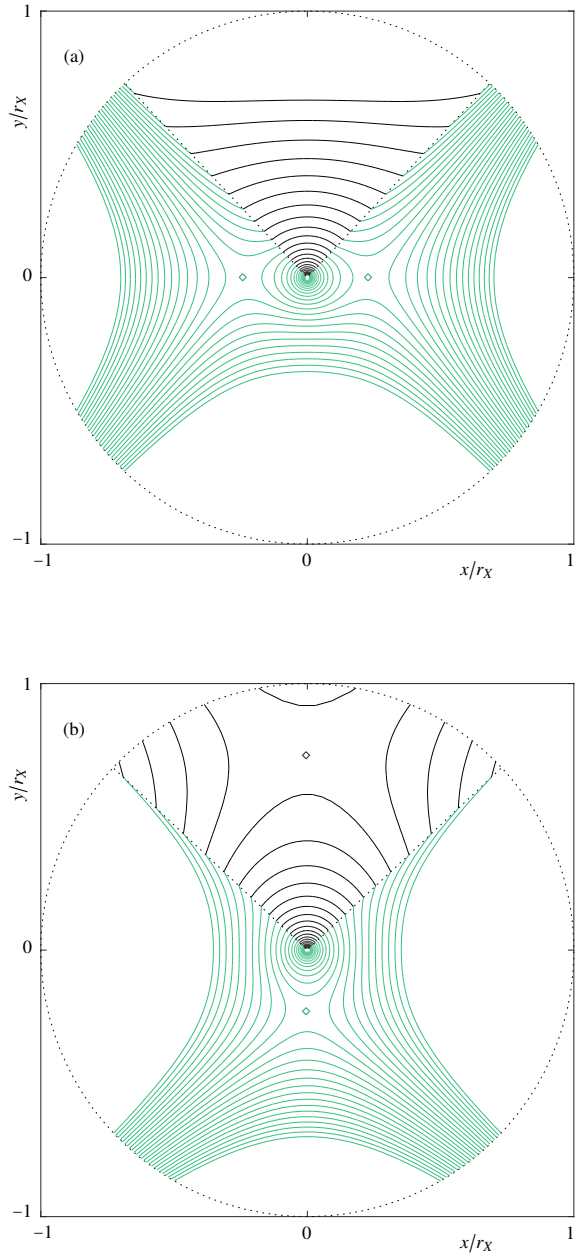

FIG. 8. Pressure contours by (14) at 25 equally distributed values in the range $[p_P\ p_X]$ near the singularity $\theta_2 - \theta_1 = \pi/2$. (a) $\theta_1 = 0.26\pi$, $\theta_2 = 0.74\pi$. (b) $\theta_1 = 0.24\pi$, $\theta_2 = 0.76\pi$. $k_1 = 1\mathrm{e}-07\mathrm{m}^2$ (green / grey), $k_2 = 1\mathrm{e}-06\mathrm{m}^2$ (black). Diamonds mark saddle points. Note that the saddle points lie on the horizontal in (a) and on the vertical in (b). All other parameters listed in appendix A

involve no special functions and thus are much more accessible to landfill design engineers. The preparation of the contour maps requires a simple facility for solution of linear equations and plotting, both widely available. The maps allow an easy graphical estimation of the well radius of influence.

The concept of the radius of influence was historically adopted from vertical hydraulic wells extracting incompressible fluid. Due to the weak compressibility of the fluid here and logarithmic pressure growth away from the well in conjunction with small generation rates, axisymmetric solutions give the radius of influence as infinite for all practical purposes. Introduction of cut-off thresholds[12] as well as full numerical simulations in non-axisymmetric domains[17] entailed better results, nevertheless overestimating the values suggested by the experience of field operators. Application of the exact solutions herein to this problem provides more realistic estimates. A complete investigation of their quality is beyond the scope of this contribution and constitutes a topic of future studies.

That landfill medium permeability is highly variable both spatially and temporally, is a long accepted fact. The analysis carried out in this study demonstrates how this heterogeneity impacts the effectiveness of collection: the presence of one sector of an increased resistance, regardless of orientation, severely undermines the well's reach. The landfill designer or operator should strive to make the waste permeability as uniform as possible. Mathematically the homogeneity will remove undesired saddle points in the pressure contour map and preclude fluid accumulation in pockets of high resistance, circulation around the landfill cell and ultimately escape through the boundary.

A real landfill cell contains a thin supporting layer of gravel around the well, whose permeability nominally differs from that of the waste. The assumption of axial symmetry admits a solution to a flow field comprising any number of concentric annular laminae of distinct permeabilities, albeit commonly only two are used[12]. The desired operational regime of a properly constructed landfill is that the resistance of the gravel lamina does not impede gas collection. The qualitative dependence on the ratio of gravel to waste permeability can be classified as follows. With ratios greater than 0.1 (in an ideal design greater than 1, but the lamina's thinness renders one order of magnitude less still acceptable) the pressure gradient is dominant near the well, but not excessively so. For ratios beneath 0.1, as can happen when the waste density is rather low, the imposed vacuum dissipates over the gravel lamina, resulting in extremely slow flow through the waste. Combining azimuthal and radial piecewise constant permeability functions appears impossible, as all degrees of freedom are exhausted in proper coupling of the sectors' flow fields along contiguity rays. Scrutiny of contours in figures 3–7 reveals that with a single lamina the flow regime matches the regular landfill operation, whereby the presence of a gravel layer is not an imperative qualitative requirement. When modelling flow through an extremely loose medium, one should weigh the benefit of including the gravel layer and thus shifting the location of the steepest pressure gradient from the main lamina to an adjacent, yet separate layer, versus the qualitative

advantage of the asymmetry accorded by the azimuthal variation of permeability.

The interpretation oriented toward the horizontal well problem is forthwith adaptable to the vertical well. The isocontour maps in figures 3–7 then represent horizontal cross-sections of the surrounding ground. Sectors of lower permeability correspond to a denser matrix, such as compacted organic waste, finer soil or fractured rock.

The steady state flow equation (3a) possesses bifurcation points, whose presence is manifested as a singularity of the linear system of equations conforming to equations (3b) and (3c). For instance, in the case $N = 2$ the locus of bifurcation points is the line $\theta_2 - \theta_1 = \pi/2$. When "crossing" from one side of this line to the other, the solution function's saddle points abruptly move between two perpendicular lines. For $N > 2$ the loci are more complicated and their complete analysis is beyond the scope of this study. Whensoever system (3) is singular, a time dependent flow equation must be solved.

Data sharing is not applicable to this article as no new data were created or analyzed in this study.

REFERENCES

[1] P. C. Carman, Trans. Inst. Chem. Eng. **15**, 150 (1937).
[2] A. H. D. Cheng, Water Resour. Res. **20**, 980 (1984).
[3] B. C. Chandrasekhara, Wärme- und Stoffübertragung **19**, 195 (1985).
[4] B. C. Chandrasekhara and P. M. S. Namboodiri, Int. J. Heat Mass Transfer **28**, 199 (1985).
[5] D. A. S. Rees and I. Pop, Int. J. Heat Mass Transfer **43**, 2565 (2000).
[6] M. H. Hamdan and M. T. Kamel, Adv. Theor. Appl. Mech. **4**, 135 (2011).
[7] F. Capone, M. Gentile, and A. A. Hill, Acta Mechanica **216**, 49 (2011).
[8] V. Ciriello, V. Di Federico, R. Archetti, and S. Longo, Int. J. Non-Linear Mech. **57**, 168 (2013).
[9] V. K. Verma and S. Datta, Journal of Porous Media **15(10)**, 891 (2012).
[10] V. K. Verma and S. K. Singh, Spec. Top. Rev. Porous Media: Int. J. **5(4)**, 355 (2014).
[11] V. K. Verma and S. Datta, Journal of Porous Media **15(7)**, 689 (2012).
[12] Y. Nec and G. Huculak, Transport in Porous Media **130(3)**, 769 (2019).
[13] W. B. Fulks, R. B. Guenther, and E. L. Roetman, Acta Mechanica **12**, 121 (1971).
[14] S. Whitaker, Transport in Porous Media **1**, 3 (1986).
[15] A. Young, J. Environ. Eng. **115(6)**, 1073 (1989).
[16] T. A. Davidson, *A simple and accurate method for calculating viscosity of gaseous mixtures* (Report of investigations 9456, US Department of the Interior, Bureau of Mines., 1993).
[17] D. Halvorsen, Y. Nec, and G. Huculak, Phys. Chem. Earth **113**, 50 (2018).
[18] T. G. Townsend, W. R. Wise, and P. Jain, J. Environ. Eng. **131(12)**, 1716 (2005).
[19] W. R. Wise and T. G. Townsend, J. Environ. Eng. **137(6)**, 514 (2011).
[20] E. Durmusoglu, M. Y. Corapcioglu, and K. Tuncay, J. Environ. Eng. **131(9)**, 1311 (2005).
[21] L. Yu, F. Batlle, J. Carrera, and A. Lloret, J. Hazard. Mater. **168**, 1404 (2009).
[22] J. D. Hyman, S. Karra, N. Makedonska, C. W. Gable, S. L. Painter, and H. S. Viswanathan, Comp. Geosci. **84**, 10 (2015).
[23] S.-J. Feng, Q.-T. Zheng, and H.-J. Xie, Comput. Geotech. **68**, 117 (2015).

APPENDIX A. BASE PARAMETERS

Table I lists the nominal set of parameters used in examples throughout (dimensional). Negative pressure values are relative to the atmosphere.

parameter	value
inner radius	0.0762 m (3 in)
outer radius	9.0762 m
temperature	15°C
well pressure p_P	−1.25 kPa
surface pressure p_X	1 atm
generation rate C	0.05 kg/(m^{3}s)
CH_4 molar fraction	0.5
O_2 molar fraction	0.01
CO_2 molar fraction	0.4

TABLE I. Parameters of a landfill cell common to all examples

APPENDIX B. TWO UNEQUAL SECTORS: SOLUTION DETAIL

Substituting (8) into (3b) and (3c) for the contiguity ray θ_o (the second ray does not contribute independent equations due to symmetry) yields

$$-\frac{C}{2k_1}r^2 + {b_{10}}^{(1)} + {b_{20}}^{(1)}\ln r + \sum_{n=1}^{\infty}\left\{\left({a_{1_n}}^{(1)}r^{2n+1} + {a_{2_n}}^{(1)}r^{-(2n+1)}\right)\sin\left((2n+1)\theta_o\right) + \left({b_{1_n}}^{(1)}r^{2n} + {b_{2_n}}^{(1)}r^{-2n}\right)\cos\left(2n\theta_o\right)\right\} =$$

$$-\frac{C}{2k_2}r^2 + {b_{10}}^{(2)} + {b_{20}}^{(2)}\ln r + \sum_{n=1}^{\infty}\left\{\left({a_{1_n}}^{(2)}r^{2n+1} + {a_{2_n}}^{(2)}r^{-(2n+1)}\right)\sin\left((2n+1)\theta_o\right) + \left({b_{1_n}}^{(2)}r^{2n} + {b_{2_n}}^{(2)}r^{-2n}\right)\cos\left(2n\theta_o\right)\right\} \quad \text{(B1a)}$$

and

$$k_1\sum_{n=1}^{\infty}\left\{(2n+1)\left({a_{1_n}}^{(1)}r^{2n+1} + {a_{2_n}}^{(1)}r^{-(2n+1)}\right)\cos\left((2n+1)\theta_o\right) - 2n\left({b_{1_n}}^{(1)}r^{2n} + {b_{2_n}}^{(1)}r^{-2n}\right)\sin\left(2n\theta_o\right)\right\} =$$

$$k_2\sum_{n=1}^{\infty}\left\{(2n+1)\left({a_{1_n}}^{(2)}r^{2n+1} + {a_{2_n}}^{(2)}r^{-(2n+1)}\right)\cos\left((2n+1)\theta_o\right) - 2n\left({b_{1_n}}^{(2)}r^{2n} + {b_{2_n}}^{(2)}r^{-2n}\right)\sin\left(2n\theta_o\right)\right\}. \quad \text{(B1b)}$$

The terms including a_{i0}, $i = \{1,2\}$, were omitted in (B1) to facilitate the juxtaposition of the sine and cosine terms within the same sum. The legitimacy of this omission is to be substantiated hereinafter. An immediate observation is that ${b_{i0}}^{(1)} = {b_{i0}}^{(2)}$, whereupon one can define ${b_{i0}}^{(s)} \stackrel{\text{def}}{=} b_{i0}$, $i = \{1,2\}$, $s = \{1,2\}$. It is impossible to satisfy both (B1a) and (B1b) unless some of the sines and cosines vanish identically, similar to the semi-circular case, where $\theta_o = 0$. The equality $\sin\big((2n+1)\theta_o\big) = 0$ will hold if $\theta_o = \pi k_o/(2n_o+1)$ for some integer k_o, n_o such that $|\theta_o| < \pi/2$. Thus for now θ_o must be a rational multiple of π and $n_o \neq 0$. If an irrational multiple is needed, the fact that the set of rational numbers $\mathbb{Q}$ is dense within the set of real numbers $\mathbb{R}$, implies there exist k_o, n_o such that θ_o is arbitrarily close to the desired value.

If there exist indices n_* such that the equality

$$(2n_*+1)\theta_o = \pi k_*$$

holds for some integer k_*, out of the infinite sum a sequence of terms will vanish. This happens when

$$2n_*+1 = (2n_o+1)k_*/k_o.$$

The left hand side is an odd number, $2n_o+1$ is an odd number, and therefore so must be k_*/k_o. Hence $k_* = (2m-1)k_o$ for any integer $m \geqslant 1$. Then $n_* = (2m-1)n_o + m - 1$ and all terms containing $\sin\Big(\big(2n_*(m)+1\big)\theta_o\Big)$ vanish in (B1a), whereas the respective cosine terms do not. In particular, since $n_o \neq 0$, n_* cannot equal unity, thus justifying the unification of the infinite series in (B1). Similarly there is a sequence of vanishing sine terms in (B1b) for $\tilde{n}_* = m(2n_o+1)$, $m \geqslant 1$ integer. Coefficients ${a_{in}}^{(1)}$, ${a_{in}}^{(2)}$ for any $n \neq n_*$ then satisfy

$$\begin{pmatrix} 1 & -1 \\ k_1 & -k_2 \end{pmatrix}\begin{pmatrix} {a_{in}}^{(1)} \\ {a_{in}}^{(2)} \end{pmatrix} = \begin{pmatrix} 0 \\ 0 \end{pmatrix}, \tag{B2a}$$

yielding ${a_{in}}^{(s)} = 0$, $i = \{1,2\}$, $s = \{1,2\}$. For any $n \neq \tilde{n}_*$ coefficients ${b_{in}}^{(1)}$, ${b_{in}}^{(2)}$ satisfy an identical homogeneous system and thus vanish as well bar the case $i = n = 1$, because then the functional shape r^{2n} matches the generation term, giving

$${b_{11}}^{(1)} = {b_{11}}^{(2)} + \frac{C}{2\cos(2\theta_o)}\left(\frac{1}{k_1} - \frac{1}{k_2}\right) \tag{B2b}$$

and

$$k_1 {b_{11}}^{(1)} = k_2 {b_{11}}^{(2)} \tag{B2c}$$

that result in

$${b_{11}}^{(s)} = \frac{C}{2k_s\cos(2\theta_o)}, \quad s = \{1,2\}. \tag{B2d}$$

An intriguing observation is that the case $\theta_o = \pi/4$ is singular. There appears to be no solution for this case, cf. the more general case with no symmetry assumptions in appendix D. Another important inference is that the restriction on θ_o being a rational multiple of π becomes superfluous, as all higher azimuthal frequency terms were proven to vanish.

APPENDIX C. *N* ARBITRARY SECTORS: SOLUTION DETAIL

At first suppose that there exists an angle θ_o such that every contiguity ray satisfies $\theta_s = n_s\theta_o$ for some integer $n_s \geqslant 0$, to wit all sector angles are multiples of a minimal angle that might be smaller than the smallest chosen sector. Now redefine N to be $N = 2\pi/\theta_o$. Since the sum of all sectors must equal 2π and each sector is a multiple of θ_o, this definition indeed yields an integer. Further redefine the actual number of sectors to be N_o. Then a suitable solution form will be

$$P^{(s)} = \frac{C}{2k_s}r^2\Big(a^{(s)}\sin(2\theta) + b^{(s)}\cos(2\theta) - 1\Big) + {b_{10}}^{(s)} + {b_{20}}^{(s)}\ln r + \sum_{n=1}^{\infty}\left\{\Big(a_1{}_n^{(s)}r^{nN} + a_2{}_n^{(s)}r^{-nN}\Big)\sin(nN\theta) + \Big(b_1{}_n^{(s)}r^{nN} + b_2{}_n^{(s)}r^{-nN}\Big)\cos(nN\theta)\right\}, \quad s = \{1,\ldots,N_o\}. \tag{C1}$$

By the solution in appendix B the term of the functional shape $r^2\cos(2\theta)$ is required to balance generation, however here $r^2\sin(2\theta)$ must also be present in order to relax the constraint of symmetry tacitly present in a two sector configuration. When $N = 2$ the sum effectively starts from $n = 2$, as the terms with $n = 1$ will already have been included explicitly. Substitution of (C1) into (3b) and (3c) forthwith implies $b_{i0}^{(s)}$ are equal in all sectors, so the superscript might be omitted: $b_{i0}^{(s)} \stackrel{\text{def}}{=} b_{i0}$, $i = \{1,2\}$. Next observe that $\sin(nN\theta_s) = \sin(2\pi n n_s) = 0$, whereas $\cos(nN\theta_s) \neq 0$, whereby ${b_{in}}^{(s)}$ are equal in all sectors as well. Hence ${b_{in}}^{(s)} \stackrel{\text{def}}{=} b_{in}$, $i = \{1,2\}$, remain degrees of freedom. Equation (3c) gives

$$k_s {a_{in}}^{(s)} = k_{s+1}{a_{in}}^{(s+1)}, \quad s = \{1,\ldots,N_o\}, \tag{C2}$$

where the index $s+1$ wraps to 1 for $s = N_o$. Although not as immediate as with the coefficients b_{in}, this nevertheless is a homogeneous degenerate system with a single degree of freedom, so that ${a_{in}}^{(s)} = \Big(k_s\Big/k_1\Big)a_{in}$, where $a_{in} = {a_{in}}^{(1)}$, $i = \{1,2\}$,

remain degrees of freedom.

Finally the coefficients $a^{(s)}$ and $b^{(s)}$ satisfy a linear system of equations of size $2N_o \times 2N_o$:

$$\mathfrak{C}\boldsymbol{c} = \boldsymbol{r}, \tag{C3a}$$

wherein the matrix $\mathfrak{C}$ is almost block bi-diagonal:

$$\mathfrak{C} = \begin{pmatrix} \mathfrak{A}_1 & \mathfrak{B}_1 & & & \\ & \mathfrak{A}_2 & \mathfrak{B}_2 & & \\ & & \ddots & \ddots & \\ & & & \mathfrak{A}_{N_o-1} & \mathfrak{B}_{N_o-1} \\ \mathfrak{B}_{N_o} & & & & \mathfrak{A}_{N_o} \end{pmatrix}, \tag{C3b}$$

with each block a 2×2 matrix:

$$\mathfrak{A}_s = \begin{pmatrix} \sin(2\theta_s) & \cos(2\theta_s) \\ \cos(2\theta_s) & -\sin(2\theta_s) \end{pmatrix},$$

$$\mathfrak{B}_s = \begin{pmatrix} -k_r^{(s)}\sin(2\theta_s) & -k_r^{(s)}\cos(2\theta_s) \\ -\cos(2\theta_s) & \sin(2\theta_s) \end{pmatrix}, \quad s = \{1, \ldots, N_o\}. \tag{C3c}$$

The unknown and right hand side vectors are arranged as follows:

$$\boldsymbol{c} = \begin{pmatrix} a^{(1)} \\ b^{(1)} \\ \vdots \\ a^{(N_o)} \\ b^{(N_o)} \end{pmatrix}, \qquad \boldsymbol{r} = \begin{pmatrix} 1-k_r^{(1)} \\ 0 \\ \vdots \\ 1-k_r^{(N_o)} \\ 0 \end{pmatrix}, \tag{C3d}$$

with $k_r^{(s)} = k_s \big/ k_{s+1}$, and as before the index $s+1$ wraps back to 1 for $s = N_o$, whereby the block $\mathfrak{B}_N$ appears in the bottom left corner of $\mathfrak{C}$. System (C3a) possesses a unique solution if and only if $\det\mathfrak{C} \neq 0$. It was shown in appendix B that the analysis utilising symmetry across the vertical eventuated in a singularity in the configuration with $\theta_1 = \pi/4$ and $\theta_2 = 3\pi/4$. The current more general solution invites the question whether the additional sine term might help circumnavigate the problem. This, as well as the concomitant matter whether this is the only singularity, is resolved in appendix D.

The only unattended issue is that the coefficients a_{in}, b_{in} remained undetermined. If the boundary conditions do not contain any higher azimuthal frequencies, it is possible to set $a_{in} = b_{in} = 0$ for $i = \{1,2\}$ and $n \geqslant 1$. Consequently the assumption on the existence of a minimal sector becomes superfluous, whence N_o might be replaced with N, which is done in (16).

APPENDIX D. TWO ARBITRARY SECTORS: COMPLETE SINGULARITY ANALYSIS

The sole way of gleaning all singular configurations is to compute $\det\mathfrak{C}$ in (C3b) analytically in the hope the resulting expression is insightful without further numerical analysis. For the case $N = 2$ this is a full matrix of size 4×4. In order to attain a manageable result, algebraic manipulation is performed as follows. Multiply $\mathfrak{C}$ by an auxiliary matrix on the right:

$$\begin{pmatrix} \mathfrak{A}_1 & \mathfrak{B}_1 \\ \mathfrak{B}_2 & \mathfrak{A}_2 \end{pmatrix}\begin{pmatrix} \mathrm{I}_{2\times2} & 0_{2\times2} \\ -\mathfrak{A}_2^{-1}\mathfrak{B}_2 & \mathrm{I}_{2\times2} \end{pmatrix} = \begin{pmatrix} \mathfrak{A}_1 - \mathfrak{B}_1\mathfrak{A}_2^{-1}\mathfrak{B}_2 & \mathfrak{B}_1 \\ 0_{2\times2} & \mathfrak{A}_2 \end{pmatrix}, \tag{D1}$$

where $\mathrm{I}_{m\times m}$ and $0_{m\times m}$ denote the identity and zero matrices of indicated sizes. All blocks in $\mathfrak{C}$ are invertible. The determinant of the auxiliary matrix is unity. Therefore

$$\det\mathfrak{C} = \det(\mathfrak{A}_2)\det\left(\mathfrak{A}_1 - \mathfrak{B}_1\mathfrak{A}_2^{-1}\mathfrak{B}_2\right) =$$

$$\det(\mathfrak{A}_2)\det(\mathfrak{B}_1)\det\left(\mathfrak{B}_1^{-1}\mathfrak{A}_1 - \mathfrak{A}_2^{-1}\mathfrak{B}_2\right). \tag{D2}$$

In the derivation below $k_r = k_1/k_2$. Elementary computation now gives

$$\det(\mathfrak{A}_2) = -1, \qquad \det(\mathfrak{B}_1) = -k_r, \tag{D3}$$

$$\mathfrak{B}_1^{-1}\mathfrak{A}_1 = \begin{pmatrix} -\dfrac{1}{k_r}\sin^2(2\theta_1) - \cos^2(2\theta_1) & \left(1-\dfrac{1}{k_r}\right)\sin(2\theta_1)\cos(2\theta_1) \\ \left(1-\dfrac{1}{k_r}\right)\sin(2\theta_1)\cos(2\theta_1) & -\dfrac{1}{k_r}\cos^2(2\theta_1) - \sin^2(2\theta_1) \end{pmatrix}, \tag{D4}$$

and $\mathfrak{A}_2^{-1}\mathfrak{B}_2$ comes out equal to $\mathfrak{B}_1^{-1}\mathfrak{A}_1$ upon mapping $\theta_1 \longmapsto \theta_2$. Thence

$$\det\left(\mathfrak{B}_1^{-1}\mathfrak{A}_1 - \mathfrak{A}_2^{-1}\mathfrak{B}_2\right) = \left(\frac{1}{k_r}\Big(\sin^2(2\theta_2) - \sin^2(2\theta_1)\Big) + \cos^2(2\theta_2) - \cos^2(2\theta_1)\right)\times$$

$$\left(\frac{1}{k_r}\Big(\cos^2(2\theta_2) - \cos^2(2\theta_1)\Big) + \sin^2(2\theta_2) - \sin^2(2\theta_1)\right) - \frac{1}{4}\left(1-\frac{1}{k_r}\right)^2\Big(\sin(4\theta_1) - \sin(4\theta_2)\Big)^2 = -\left(1-\frac{1}{k_r}\right)^2\sin^2\Big(2(\theta_1-\theta_2)\Big). \tag{D5}$$

The last transition ensues upon breaking all differences of squares into products and utilising trigonometric identities. Thus $\det \mathfrak{C} = 0$ if and only if $\theta_2 - \theta_1 = \pi/2, \pi$. The case $\theta_2 - \theta_1 = \pi$ corresponds to the semi-circular configuration that was solved separately. The case $\theta_2 - \theta_1 = \pi/2$ is a persistent singularity, leaving the only conclusion that no separation of variables solution exists for any configuration, where one sector is of a right angle.

Figure 8 depicts typical pressure contours near this singularity. Scrutiny thereof reveals that the saddle points “jump" to a perpendicular line, indicating a bifurcation. Since the governing equations (3) are linear in p^2, any solution (for given boundary conditions) must be unique, and therefore this structural singularity cannot be circumnavigated via a different solution form or technique other than the separation of variables. That could have been possible only if near the singularity the solutions approached a limit that escaped the description used herein. To paraphrase, if the contours in figure 8(a) or any other configuration of that type, such as those in figure 5, were continuously deformable into those in 8(b) or similar (figures 3 and 4), said limit would have existed. Hence for the configuration of two sectors, one of which is right angled, no solution to (3) exists and the flow is expected to be non-steady.